Composite Structures 242 (2020) 112194

Contents lists available at ScienceDirect

Composite Structures

journal homepage: www.elsevier.com/locate/compstruct

Effect of fibre architecture on tensile pull-off behaviour of 3D woven composite T-joints

Shibo Yan[a,*], Xuesen Zeng[b], Andrew Long[a]

[a] Composites Research Group, Faculty of Engineering, University of Nottingham, Nottingham NG7 2RD, UK
[b] Centre for Future Materials, University of Southern Queensland, Toowoomba 4350, Queensland, Australia

ARTICLE INFO

Keywords:
3D woven composites
T-joints
Fibre architecture
Mechanical properties

ABSTRACT

3D woven composites are frequently employed due to their improved through-thickness properties and high damage tolerance compared with laminated composites. Due to the large design space for 3D weave patterns, an in-depth understanding of the relationship between the weave parameters and mechanical properties is essential for the design of these materials. This numerical study investigates the effect of fibre architecture on the mechanical performance of 3D woven composite T-joints under tensile pull-off loading. Six weave pattern variations, subjected to the same preform manufacturing constraint, are designed and numerically analysed, along with another two that have been manufactured and tested for validation previously. Results show a significant architecture dependence in the mechanical responses. Following the design of experiments on weave patterns, the complex architecture-dependant effect is decoupled by two independent variables, yarn path entanglement and yarn path crossover. The study also provides design recommendations for 3D woven T-joint reinforcements under tensile pull-off loading.

1. Introduction

3D woven composites have recently been employed for weight reduction and high performance in the aerospace applications where laminated composites cannot meet the requirements due to low interlaminar strength. For instance, the applications of 3D woven composites in the fan blades of LEAP engine [1] demonstrate the advantages of these materials, including improved through-thickness properties, high delamination resistance and near net shape manufacturing.

The design space of 3D woven composites is large, specifically for those with geometric features, as the design variables are not only orientations and thicknesses, but also an enormous variation in the 3D fibre architectures. It is fundamental at the material design phase to understand the influence of the fibre architecture of 3D woven composites on their mechanical properties. Much work has been conducted to characterise the mechanical behaviour of 3D woven composites [2–7], particular in comparison with 2D laminates, which have demonstrated their advantages in the through-thickness properties. According to the binder yarn path, 3D woven composites are usually classified into three categories: 1) orthogonal, 2) layer to layer, and 3) angle interlock. Based on the three categories, a significant amount of other variations (simply by varying binder paths) are also available. The effects of binder yarn variations on the tensile, compressive, and flexural behaviour at the coupon level were investigated by [7–16]. The binder yarn architecture affects the void content, yarn crimp (waviness) as well as a number of mechanical behaviour of the 3D woven composite [9]. Crimp in the load-carrying yarns of 3D woven composites caused by binder yarns links to the reduction of tensile modulus and strength due to the high anisotropy in fibre properties [17]. This is also supported by the studies in [9,15] as 3D orthogonal woven composite panels were found to show greater strength and modulus than angle interlock weaves in tension and compression as they have less yarn waviness. Pankow and colleagues found that layer to layer weaves exhibited plastic-like behaviour while orthogonal weaves showed very little plasticity [18]. In addition, for each types of 3D woven composites, the different ratio and spacing of binders also led to different responses in failure mechanisms in the out-of-place direction [12].

The effect of fibre architecture on the mechanical behaviour of 3D woven composite (sub-) structures are far more complex than those at the coupon level. Soden et al. [19] assessed the influence of variations in the through-thickness reinforcement of 3D woven composite T-shaped specimens on the mechanical behaviour under in-plane tensile loading. Although weave variations in the 3D woven T-joint specimens were limited to the proportion of through-thickness yarns, significant differences were shown from the tensile test results. In general, the peak

* Corresponding author.
E-mail address: shibo.yan@nottingham.ac.uk (S. Yan).

https://doi.org/10.1016/j.compstruct.2020.112194
Received 2 January 2020; Accepted 10 March 2020
Available online 14 March 2020

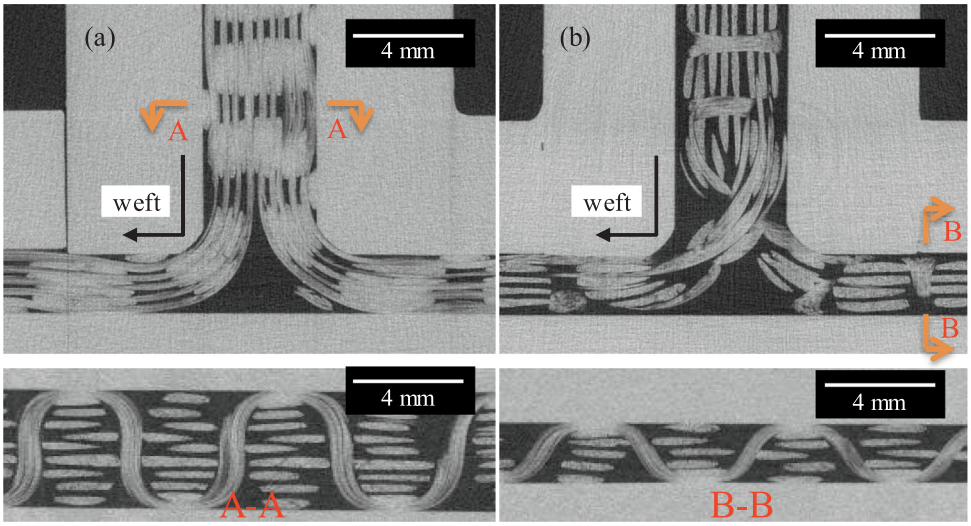

Fig. 1. Images from μCT scan of the two types of 3D preform showing the weave variation at the junction: (a) type 1 (3Dv1); (b) type 2 (3Dv2); section views show the weave pattern (orthogonal) at web and flange.

failure load increases with increasing level of through-thickness yarns. The weave variations were shown to affect the failure mode of the specimens but they concluded that the relationship was complex. In another study by the current authors [20], a weave variation in weft yarn path at the junction of the 3D woven T-joints, resulting from opening different sheds when inserting weft yarns, led to a significant difference in the mechanical performance, e.g. a more than 100% difference in the ultimate strength through the tensile pull-off tests on two types of T-joint (Fig. 1, named 3Dv1 and 3Dv2 hereafter). The manufacture process for the T-joint preforms enabled weave variations in the weft yarn path at the junction, in addition to in proportion of binders.

With the aim to optimise the weave pattern of 3D woven T-joints, further to the two experimentally tested weave patterns [20], this paper presents a comprehensive numerical study to investigate the effect of 3D reinforcement architecture on the mechanical behaviour of 3D woven T-joints under pull-off loading. Even though the weave variation is limited to the weft yarns path at the junction, which was a manufacturing constraint (Section 2), the number of possible manufacture weave patterns is still enormous. To simplify the design space, two new design variables accounting for weft yarn geometric features are proposed, based on a classification of the manufacture weave patterns (Section 3). In order to understand the influence of each proposed design variable, all the new weave patterns (Section 4) are determined by the proportion of each design variable and are evaluated through a series of simulations (Section 5). Results are compared and analysed in detail in Section 6 and recommendations for design of 3D woven T-joint reinforcements under tensile pull-off loading are given in Section 7.

2. Materials and manufacture

The two types of 3D woven T-joint preform previously tested were manufactured by Sigmatex UK from Hexcel IM7 12K carbon fibre (fabric areal density 3170 g/m^2). Specimens were woven flat with pre-positioned bifurcations on a Jacquard machine and then folded into a T shape before the vacuum resin transfer moulding process [20]. The preforms were based on a 3D orthogonal weave pattern with the only variation at the junction. This variation was only in the weft yarn path resulting from opening different sheds when inserting weft yarns at the junction, which is a typical manufacturing method for 3D woven T-joint preforms and is considered as a manufacturing constraint in this study. Schematic weave pattern in Fig. 2 highlights the weft yarn path variation, where half of the weft yarns of type 2 (hereafter named 3Dv2) are crossing over the other half at the junction, in comparison with type 1 (hereafter named 3Dv1). Both 3D woven preforms consist of 8 layers of warp yarns and 9 layers of weft yarns in the web and 4 layers of warp yarn and 5 layers of weft yarns in the flange. A weft layer in the web (numbered as 4′(5′) in Fig. 2) is formed of twofold weft yarns as used in other layers and separated into two layers (layer 4′ and 5′) at the flange, for the purpose of yarn layer balance in the flange. More details of the 3D woven preforms are given in [21].

3. Geometry-based design variables

In the current study, the design variable was restricted to only the path of the weft yarns at the junction of the T-joints. This maintains quasi-constant fibre volume fraction and does not require any modification on the weaving machine (same manufacturing constraint) that produced the preforms for the T-joint specimens previously tested. Even under such assumption, the number of variations still could be up to 3.6 million (10 factorial (10!) from permutation of 10 weft yarns). This huge number of candidates plus the high computational cost for each entry would make the evaluation of weave pattern effect difficult. In this work, we proposed two geometry-based design variables to simplify the design space. Yarn path entanglement and yarn path cross-over are introduced by a classification of the weft yarn path at the junction.

3.1. Yarn path entanglement

In typical orthogonal weaves, yarns (except binder yarns) at neighbouring layers are parallel and stacked on each other in the form of a UD laminate, with an advantage of largely reduced crimp in the yarn path. In the T-joint fibre architectures, when the neighbouring weft yarns are not parallel to each other throughout the preform (from web through radius to flange), they are entangled together at the radius by switching layers (similar to braiding) and this is referred to as yarn path entanglement. An example can be found in the paths of weft yarns number 1 to 5 of 3Dv2 model as the layer sequence in the web is different to that in the flange (Fig. 2). Yarn path entanglement defined between at least two neighbouring weft yarns is complimentary or mutually exclusive to the original yarn path parallelism in a 3D orthogonal weave. It changes the geometric feature of the weft yarns from a laminate-like to an braiding-like fibre architecture, which is less vulnerable to failure when subjected to loading in the through-thickness direction.

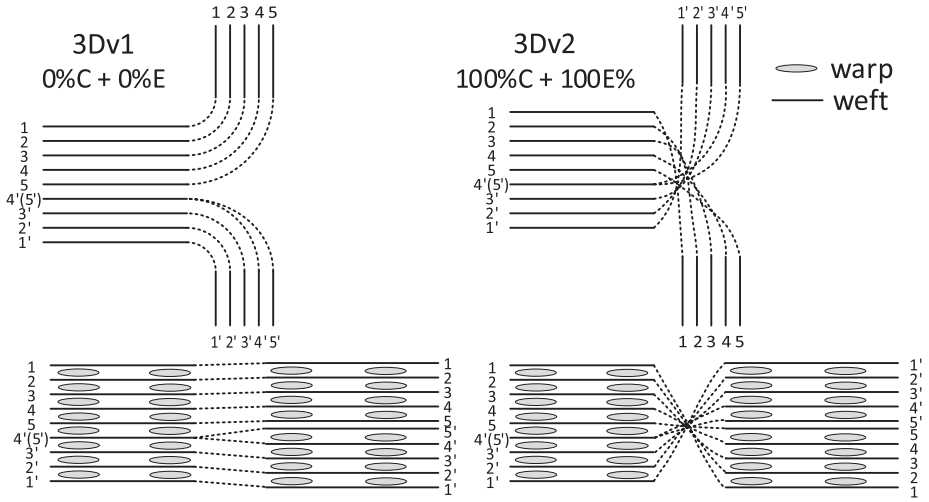

Fig. 2. Schematic weave pattern of 3Dv1 (left), 3Dv2 (right) highlighting design variable proportions.

3.2. Yarn path cross-over

The preform reinforcing the 3D woven composite T-joint was initially woven flat and then folded into a T shape before moulding, with an equal number of weft yarns in each half of the preform. If a weft yarn does not always stay in the same half of the preform, i.e. it goes across to the other half of the preform when it comes to the flange, it is referred to as yarn path cross-over. An example can be found in the 3Dv2 model illustrated in Fig. 2. Yarn path cross-over determines the fibre architecture and further influences the stress distribution around the noodle area (resin pocket at the junction).

4. Quantification of weft yarn path variations and new weave patterns

After categorizing the geometric arrangement of the weft yarns at the junction, new weave pattern variations for the T-joint can be quantified by the proportions of the basic design variables introduced above. Yarn path entanglement and cross-over are two independent design variables for the preform. Consequently, quantification of a weave pattern variation can be addressed by specifying the proportions of weft yarns in the design variable categories through the following notation: (_%C, _%E), in which %C denotes the proportion of weft yarns that have yarn path cross-over; %E denotes the proportion of weft yarns that have yarn path entanglement. For instance, as shown in Fig. 2, the weave pattern for 3Dv1 T-joint does not have yarn path cross-over and entanglement, so it can be described as (0%C + 0%E). Similarly, the weave pattern for 3Dv2 T-joint is denoted by (100%C + 100%E), as all the weft yarns have crossed over to the other half and entangled among one another.

Six new weave patterns for the 3D woven T-joint were designed, by varying the path of weft yarns at the junction. As the weave patterns for 3Dv1 and 3Dv2 specimens are the two endpoints of the proportion intervals of yarn path cross-over and entanglement, the design of new weave patterns aims to decouple the two design variables, by varying only one design variable at a time, to determine the effect of each single variable on the mechanical performance. It is noted that random distribution of the proportions of design variables is not considered, but here weave patterns were designed by covering some selected proportions of the design variables. All variations were quantified by the proportions of yarn path entanglement and yarn path cross-over. The six new weave patterns were named 3Dv3 to 3Dv8, and the schematic weave patterns showing the weave variations can be found in Fig. 3. Note that a simple way to track the change of weft yarn path is to compare the numbering of the weft yarns (1 to 5, and 1′ to 5′) at the web with those at the flange of the preform.

5. Virtual testing

A meso-scale modelling method was proposed by the authors to simulate the 3D woven fibre architectures and the mechanical performance of the composite T-joints, subjected to quasi-static tensile pull-off loading [22]. The method was shown to be predictive as no input data correlation was required in the damage model for the two previously tested specimens (Fig. 1), whose weave variations were restricted to the junction as in this paper. The fibre architectures of the 6 newly designed 3D woven T-joint were created in TexGen (Fig. 4). Based on the yarn path defined in the weave patterns (Fig. 3), the weft yarns at the junction of the TexGen models were assumed to have the same cross-sections to 3Dv1 or 3Dv2 models in terms of design variables. For examples, the weft yarns of 3Dv3 model have the same cross-sections to the 3Dv1 model as both of their weft yarns are considered as yarn path parallelism. Outside the junction part of the T-joint models the architectures are the same among all weave patterns (regions by solid lines in Fig. 3). The modelling strategy for the geometric models is illustrated in Fig. 4.

The T-joint models were numerically tested through validated simulation in [22], and all material properties are consistent with those used for the T-joint specimens. Damage modelling incorporated both yarn/matrix interface damage and damage in bulk matrix and homogenized yarn materials, in conjunction with a continuum damage mechanics (CDM) approach to account for the progressive failure behaviour. The quadratic stress criterion and mixed mode power law were selected for interface damage initiation and evolution:

$$\left\{\frac{\langle \tau_n \rangle}{\tau_n^0}\right\}^2 + \left\{\frac{\tau_s}{\tau_s^0}\right\}^2 + \left\{\frac{\tau_t}{\tau_t^0}\right\}^2 = 1 \tag{1}$$

$$\left\{\frac{G_n}{G_n^C}\right\}^p + \left\{\frac{G_s}{G_s^C}\right\}^p + \left\{\frac{G_t}{G_t^C}\right\}^p = 1 \tag{2}$$

where τ^0 is the initial failure stress, G^C is critical energy release rate for each of the single delamination modes, with subscript stands for normal, first and second shear directions; and p is the power in the criterion. ‘ < > ’ is the Macaulay operator.

For damage in the homogenized yarn material, Hashin’s failure criteria [23] developed for UD composites were used here to capture the damage initiation for each failure mode:

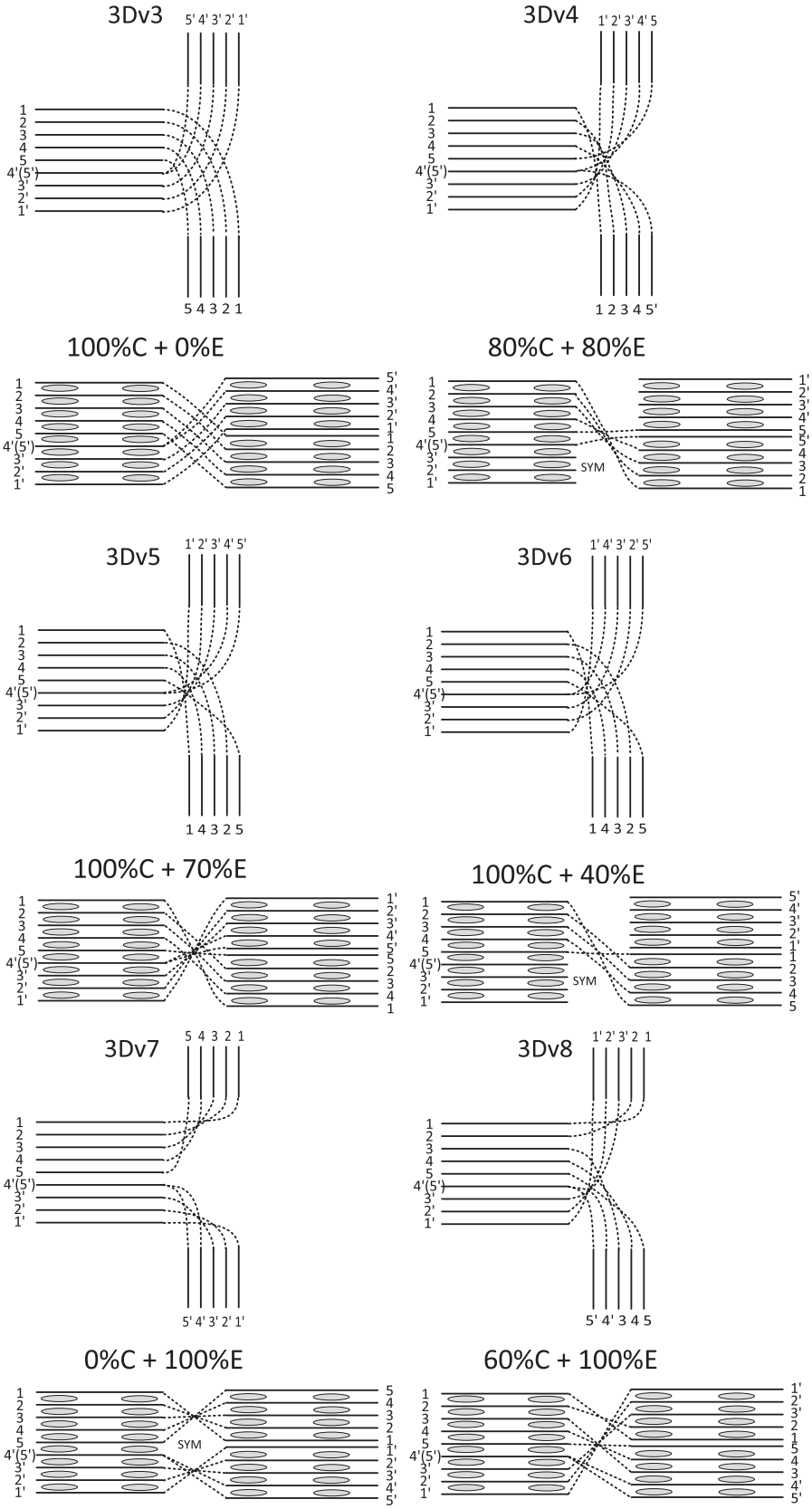

Fig. 3. Schematic weave pattern of 3Dv3 to 3Dv8 (right) highlighting design variable proportions.

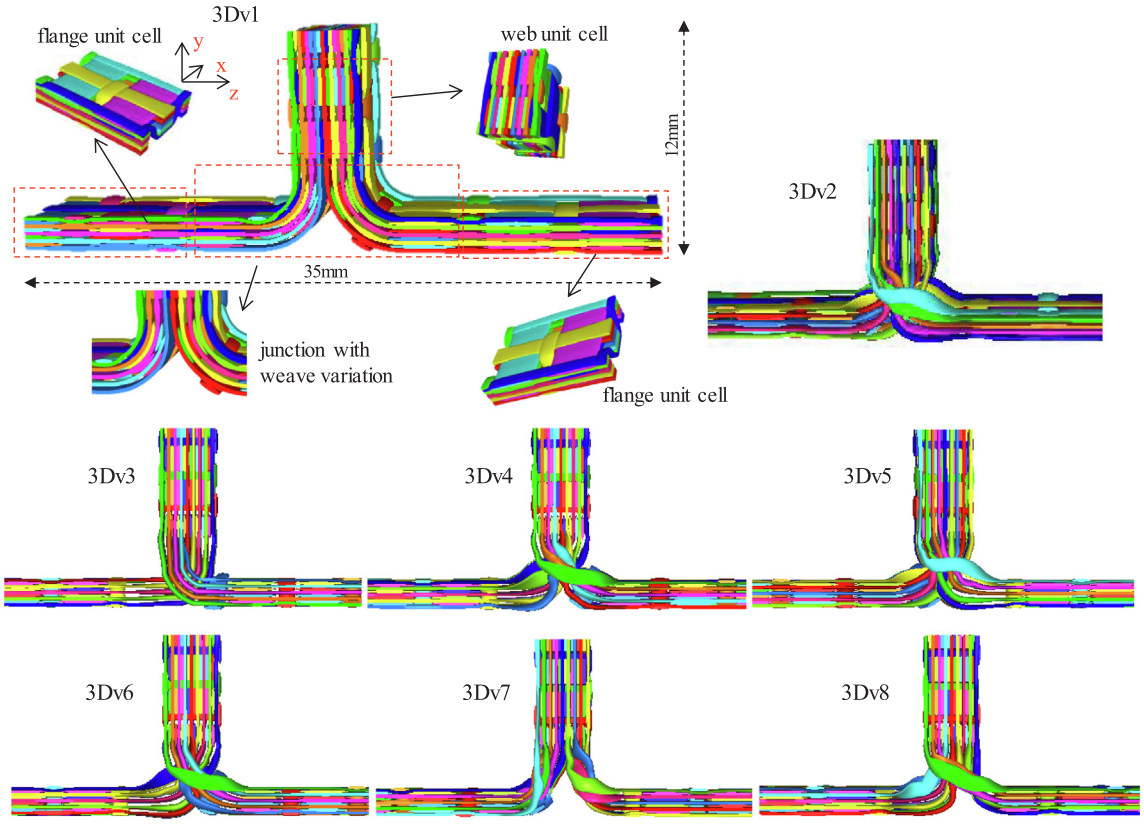

Fig. 4. Reinforcement geometric models built in TexGen for 3Dv1 to 3Dv8 T-joints; flanges and webs are of the same fibre architectures among the eight designs.

$$I_1 \geqslant 0:\ \mathrm{d}_1 = \left(\frac{I_1}{F_1^t}\right)^2 + \frac{I_4}{F_{12}^2} = 1,\quad I_1 \leqslant 0:\ d_2 = \left(\frac{I_1}{F_1^c}\right)^2 = 1;$$
$$I_2 \geqslant 0:\ d_3 = \left(\frac{I_2}{F_2^t}\right)^2 + \frac{I_3}{F_{23}^2} + \frac{I_4}{F_{12}^2} = 1,\quad I_2 \leqslant$$
$$0:\ d_4 = \left[\left(\frac{F_2^c}{2F_{23}}\right)^2 - 1\right]\left(\frac{I_2}{F_2^c}\right) + \left(\frac{I_2}{2F_{23}}\right)^2 + \frac{I_3}{F_{23}^2} + \frac{I_4}{F_{12}^2} = 1;$$
$$I_1 = \sigma_1;\ I_2 = \sigma_2 + \sigma_3;\ I_3 = \tau_{23}^2 - \sigma_2\sigma_3;\ I_4 = \tau_{12}^2 + \tau_{13}^2 \tag{3}$$

where I_1 to I_4 are the four stress invariants; d_1 and d_2 are the damage parameters for fibre dominated failure modes; d_3 and d_4 are the damage parameters for transverse matrix dominated failure modes. Bulk matrix damage was evaluated by the pressure dependent modified von Mises criterion which can take into account the difference between tensile and compressive strength for the isotropic material [24]:

$$d_m = \frac{F_m^c - F_m^t}{F_m^c F_m^t}(\sigma_1 + \sigma_2 + \sigma_3) + \frac{1}{2F_m^c F_m^t}[(\sigma_1 - \sigma_2)^2 + (\sigma_2 - \sigma_3)^2 + (\sigma_1 - \sigma_3)^2] \tag{4}$$

where F_m^c, F_m^t are the compressive and tensile strengths of the bulk matrix respectively.

After damage initiation, the behaviour of the damaged constituent materials was modelled by a CDM approach [25]:

$$P(d_i) = \left(1 - \frac{1}{\exp(-c_1 d_i + c_2)}\right) \tag{5}$$

where $P(d_i)$ is a stiffness penalty factor function for degrading the corresponding modulus in terms of the failure modes d_i defined in Eq. (3) and (4). c_1 and c_2 are constants. Thus the elastic properties of the damaged yarn material are:

$$E_1^d = E_1 coef_1 \qquad E_2^d = E_3^d = E_2 coef_1 coef_2$$
$$G_{12}^d = G_{13}^d = G_{12} coef_1 \quad G_{23}^d = G_{23} coef_1 coef_2$$
$$coef_1 = \begin{cases} max(0.001, P(d_1)) & d_1 \geqslant 1 \\ 0.001 & d_2 \geqslant 1 \end{cases}$$
$$coef_2 = max(0.001, min(P(d_3), P(d_4))) \tag{6}$$

where E, G with superscript d denote the moduli of the damaged yarn material. A minimum value of 0.001 for the stiffness penalty factor $P(d_i)$ was maintained when the material is fully damaged to avoid numerical instability. Similarly, the Young's modulus of the damaged bulk matrix material is:

$$E_m^d = E_m \max(0.001, P(d_m)) \tag{7}$$

where E with superscript d denotes the Young's modulus of the damaged matrix material.

FE models were solved by Abaqus Explicit 6.13 with a user-defined material subroutine (VUMAT).

6. Results

The predicted results of the six new 3D woven T-joint models along with those of the 3Dv1 and 3Dv2 models were compared together in terms of structural stiffness and load carrying capacity. Due to the existence of nonlinearity in the structural stiffness, the stiffness is defined at a displacement of 0.35 mm, at which stage macroscopic damage has not yet initiated. The load carrying capacity is defined between 1.5 mm and 1.6 mm in displacement, to capture the responses after damage initiation given that ultimate failure load is likely to be unreliable from the simulations.

The stiffnesses and load carrying capacities defined above of all 8 T-joint models are plotted in Fig. 5 with 3Dv1 and 3Dv2 validated against experimental results. An illustration for the definition of the compared structural stiffness and load carrying capacity of the T-joint models is

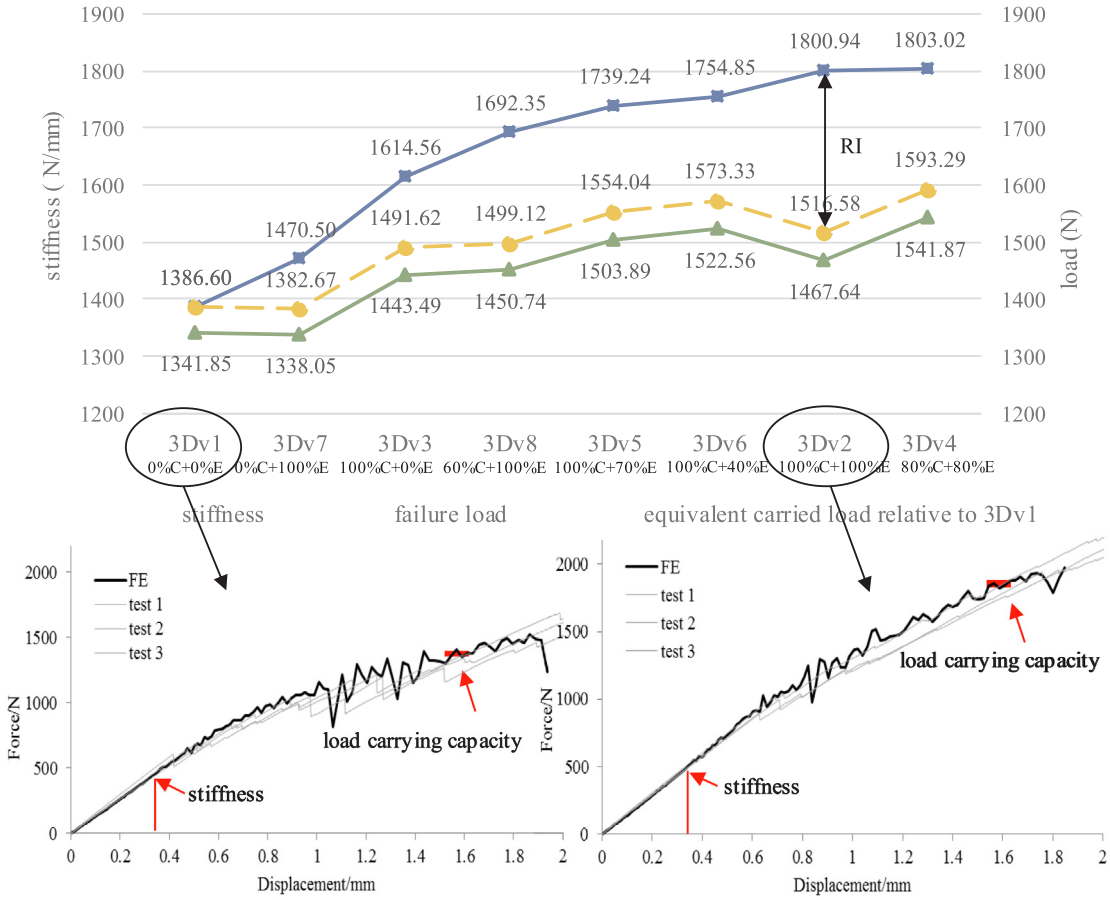

Fig. 5. Top: Comparison of predicted structural stiffness and load carrying capacity of the 3D woven T-joint models; bottom left: response of 3Dv1 model validated against experimental results; bottom right: response of 3Dv2 model validated against experimental results.

given in Fig. 5 (bottom). Distinct differences in the stiffness and load carrying capacity are shown among these 3D woven T-joint models with only weave variations at the junction. The maximum difference in the stiffness, i.e. between 3Dv7 and 3Dv4, is 15.2%, whilst the maximum difference in the carried load, i.e. between 3Dv1 and 3Dv4, is 30.0%. Note that in the experiment the ultimate strength of 3Dv2 can be 100% more than that of 3Dv1 [20]. In addition, the influence of fibre architecture on stiffness is not as significant as that on load carrying capacity. The varied mechanical behaviour resulting from these variations in the fibre architectures demonstrated that the performance of 3D woven composites can be tailored, which is an advantage of such materials but techniques that can predict the resulting structural performance are also needed at the design stage.

6.1. Damage resistance of the 3D woven T-joint models

As there is only a minor difference in the initial stiffness of the T-joints, the ultimate strength of the T-joints is mostly dominated by the damage resistance capability. At a displacement of around 1.5 mm, which is beyond damage initiation but not close to that for the ultimate strength as observed in the experiments for 3Dv1 and 3Dv2 [20], the defined load is still partially affected by the inherent stiffness (although a minor difference), rather than solely reflecting the damage resistance capability. If a T-joint model is inherently stiffer but weaker (in terms of ultimate strength) than another T-joint because of the variation in the fibre architectures, the defined load for this T-joint model could also be higher if no catastrophic damage has occurred at 1.5 mm to 1.6 mm displacement due to the elastic contribution to the load carrying capacity. A damage resistance indicator (*RI*) is defined to decouple this contribution from the defined load carrying capacity. First the equivalent carried load relative to 3Dv1 is calculated by assuming they have the same damage resistance capability as 3Dv1 but retain their own stiffness (Eq. (8)). Therefore, the difference between the defined load carrying capacity and equivalent carried load relative to 3Dv1, as illustrated in Fig. 5 (top), is the damage resistance indicator that the specific fibre architecture of each T-joint model offers.

$$CL_i^{equi} = \frac{ST_i}{ST_{3Dv1}} CL_{3Dv1}$$
$$RI_i = CL_i - CL_i^{equi} \quad (8)$$

where *CL* represents the load carrying capacity; *ST* denotes the stiffness; subscript *i* ranges from *3Dv1* to *3Dv8* denoting each T-joint model, and superscript *equi* denotes equivalent carried load to 3Dv1.

It is noted that the distribution of the *RI* of the T-joint models is largely consistent with trend for the defined load carrying capacity, except 3Dv4 which shows a noticeably lower *RI* than 3Dv2, after decoupling the stiffness contribution. This means that the slightly higher load carrying capacity of 3Dv4 is mostly due to its higher stiffness, and it may have already accumulated more damage than 3Dv2, which is likely to achieve a higher ultimate strength. Therefore, the extent of damage in terms of interface and constituent materials of each T-joint model was investigated to validate the above analysis on the effect of damage resistance indicator. The interface damage is quantified by the ratio of the number of damaged nodes, whose damage parameter (Abaqus notation: CSDMG) is greater than 0, to the total number of nodes at the interface. In addition, an interface damage ratio for damage parameter (CSDMG) greater than or equal to 0.9 (full damage occurs at the value of 1) is used to characterise the proportion of

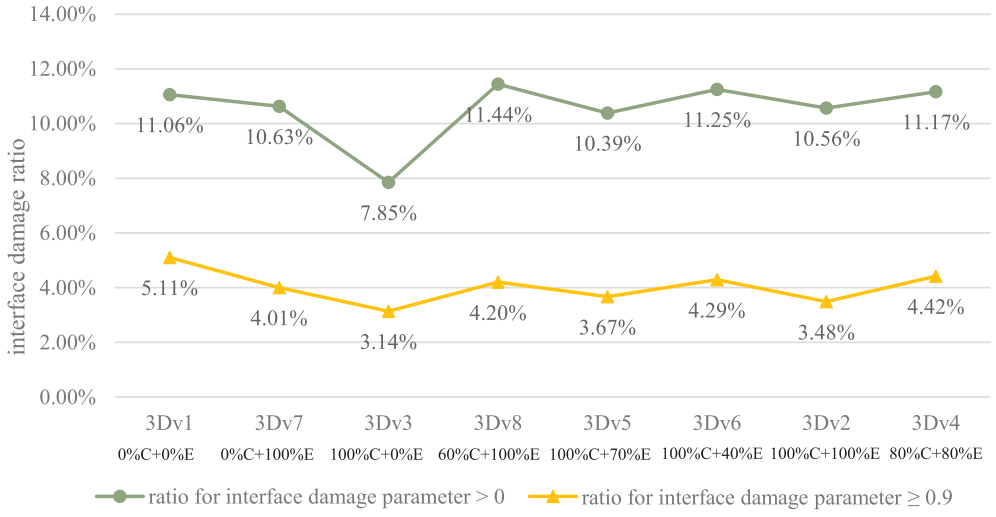

Fig. 6. Comparison of interface damage ratios in the 3D woven T-joint models at displacement of 1.57 mm.

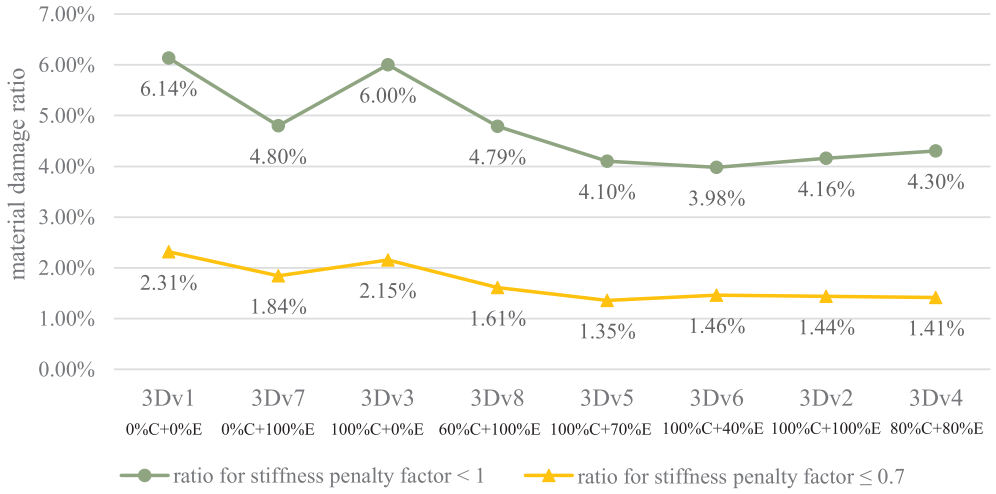

Fig. 7. Comparison of constituent material damage ratios in the 3D woven T-joint models at displacement of 1.57 mm.

severely damaged interface. Meanwhile, the constituent material damage ratio is defined as the ratio of the number of damaged matrix and yarn elements with stiffness penalty factor *P* (full damage occurs at the value of 0.001) less than 1 in terms of all types of failure modes, to the total number of elements in the model. Similarly, an additional material damage ratio for *P* less than or equal to 0.7 is employed to evaluate the proportion of the damaged materials whose moduli have be degraded to less than or equal to 70% of the values of the intact materials. Fig. 6 and Fig. 7 show the comparisons of interface damage ratios and the constituent material damage ratios of the T-joint models respectively, at the same displacement of 1.57 mm.

Based on Figs. 6 and 7, the damage extent within the T-joint model appears to be able to represent the *RI* deduced in Fig. 5. In general, a T-joint model with lower *RI* was shown to have higher damage ratios and vice versa. It is also found that the *RI* is collectively affected by damage at the interface and constituent materials. For instance, although 3Dv3 had a low percentage of interfacial damage, it did not achieve a high load due to its high damage ratio in the constituent materials. The observation that more damage accumulated in 3Dv4 than 3Dv2 as implied from the above damage resistance analysis is supported by the damage ratios.

6.2. Effects of yarn path crossover on stiffness and damage resistance

In order to determine the effects of each single design variable on mechanical performance of the T-joint models, some of the new weave patterns were designed to have the same percentage in either of the two design variables. Through analysing the results of the T-joint models which have the same proportion of yarn path entanglement but varied proportions in yarn path cross-over, the effects of yarn path crossover can be isolated. Based on all 8 T-joint models, direct comparisons can be made at the yarn path entanglement proportions of 0% and 100%.

By comparing the results of 3Dv7, 3Dv8 and 3Dv2 (Fig. 8 left) which have the same proportion of yarn path entanglement at 100% but different proportions of yarn path cross-over at 0%, 60% and 100% respectively, it is found that there is a monotonic improvement in the stiffness and damage resistance with the increase of yarn path cross-over proportion. Similarly, by comparing the results of 3Dv1 and 3Dv3 (Fig. 8 right), which have the same proportion of yarn path entanglement at 0%, but different proportions of yarn path cross-over at 0% and 100% respectively, an increasing trend is shown in the stiffness and damage resistance after improving the yarn path cross-over proportion from 0% to 100%.

Increasing the yarn path cross-over proportion of the preforms in the 3D woven T-joints was shown to improve both stiffness and damage resistance under quasi-static tensile pull-off loading, when the yarn entanglement proportion is fixed at either 0% or 100%. This is because yarn path cross-over reduces the size of the noodle as seen in those patterns without yarn cross-over by reinforcing it with the crossed weft yarns. In addition, it removes a sharp interface between the left and

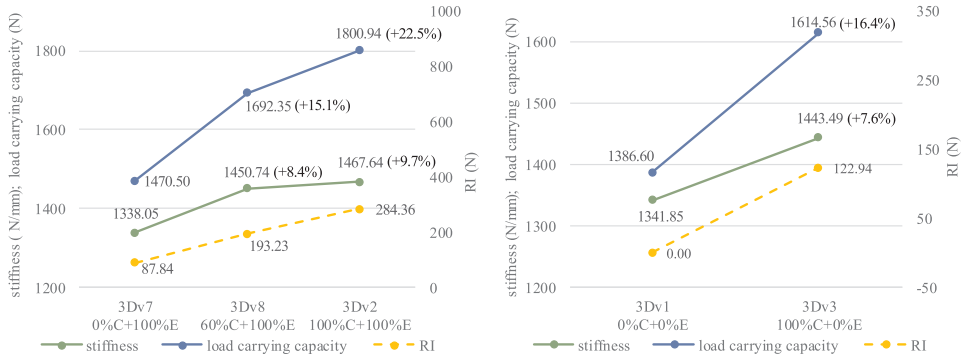

Fig. 8. Comparison of stiffness, load carrying capacity and damage resistance: left, 3Dv7, 3Dv8 and 3Dv2 T-joint models at a yarn path entanglement proportion of 100%; right, 3Dv1 and 3Dv3 T-joint models at a yarn path entanglement proportion of 0%.

right sides of the T-joint so that delamination is difficult to propagate into the web.

6.3. Effects of yarn path entanglement on stiffness and damage resistance

Similarly, the effects of yarn path entanglement on stiffness and damage resistance can be found by analysing the results of the T-joint models which have the same proportion of yarn path cross-over but varied proportions in yarn path entanglement. Based on all 8 T-joint models, direct comparisons can be made at yarn path crossover proportions of 0% and 100%.

By comparing the results of 3Dv3, 3Dv6, 3Dv5 and 3Dv2 (Fig. 9 left), which have the same proportion of yarn path cross-over at 100% but different proportions of yarn path entanglement at 0%, 40%, 70% and 100% respectively, it is shown that increasing the proportion of yarn path entanglement leads to an increase and then a decrease of stiffness. And a monotonic increase in damage resistance was observed with the increase of yarn path entanglement proportion. By comparing the results of 3Dv1 and 3Dv7 (Fig. 9 right), which have the same proportion of yarn path cross-over at 0% but different proportions of yarn path entanglement at 0% and 100% respectively, it is observed that there is a minor decrease in the stiffness but a slight increase in the damage resistance after improving the yarn path entanglement proportion from 0% to 100%.

To conclude, a monotonic increase in damage resistance was observed with the increase of the yarn path entanglement proportion, due to the entangled fibre architecture of weft yarns, in which delamination is more difficult to propagate than in a laminate-like structure. However, the noodle is still a critical failure area as yarn path entanglement does not reinforce the noodle, so the improvement in strength is not as significant as that obtained by increasing yarn path cross-over proportion. For instance, there was only a 6.1% increase in load carrying capacity when yarn path entanglement proportion was improved changed 0% to 100% (Fig. 9 right), versus a 16.4% increase for an equivalent change in yarn path cross-over proportion (Fig. 8 right). It was found that the stiffness did not always follow the increasing trend of damage resistance when increasing the yarn path entanglement proportion, as an optimum pattern for higher stiffness was found at a yarn entanglement ratio of about 40%, which is likely to be caused by yarn crimp introduced by further entanglement. This is supported by the fact that 3Dv4 had a higher stiffness than 3Dv2 after slightly reducing its yarn path entanglement proportion (by 20%) without a significant change in the proportion of the yarn path cross-over in the fibre architecture.

7. Design recommendations for 3D woven T-joint reinforcement under tensile pull-off loading

The deformation of the T-joint under tensile pull-off loading is comprised of the tensile deformation in the web and the deflection from bending of the flange. Due to the high effective modulus in the web along its loading direction, the deformation of the T-joint from tension in the web is negligible when compared with that from bending. The initial stiffness of the T-joint is thus largely determined by the T-joint flange in bending, and fibre architecture at the junction could have a minor impact on it. This is supported by the fact that a maximum difference of 15.2% was observed in stiffness among the 8 T-joint models, which have the same fibre architecture in the flange but varied pattern at the junction. Conversely, the fibre architecture at the junction dominates the failure behaviour of the T-joint under the tensile pull-off testing and could lead to a step-change in the ultimate failure load by changing the failure mode, i.e. a more than 100% increase between the two different T-joint specimens tested experimentally. Like laminated composites, the primary damage mode in the 3D woven composite T-joints under pull-off loading is delamination between the bulk matrix and yarns. A typical orthogonal weave pattern, as seen in 3Dv1, can

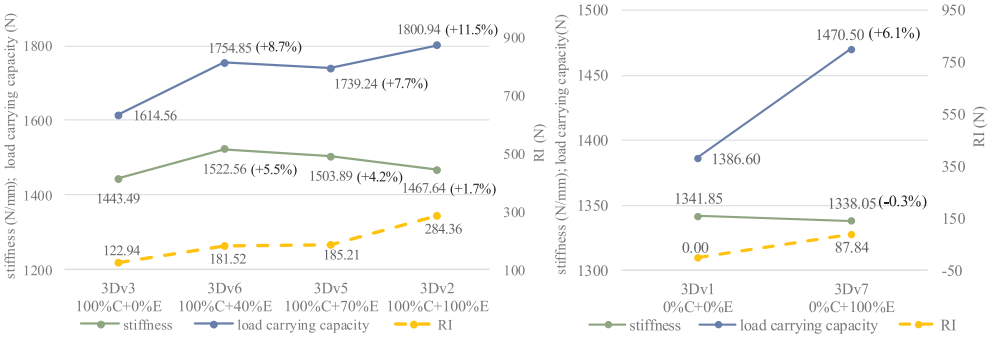

Fig. 9. Comparison of stiffness, load carrying capacity and damage resistance: left, 3Dv3, 3Dv6, 3Dv5 and 3Dv2 T-joint models at a yarn path cross-over proportion of 100%; right, 3Dv1 and 3Dv7 T-joint models at a yarn path cross-over proportion of 0%

alleviate delamination by the presence of binder yarns when compared to the equivalent laminated specimen. However, if the delamination propagation is mostly arrested by further varying the fibre architecture at the junction rather than solely relying on the binders, the damage tolerance of the composites would be significantly improved.

The weft yarns take most of the loads under this specific tensile pull-off loading case. Using yarn path cross-over in the weft yarns was found to be an effective way to improve the stiffness and damage resistance. It appears that the more yarn path cross-over being introduced, the better damage resistance capability the T-joint can gain, as the noodle would be reinforced by the crossed weft yarns. The T-joint models without yarn path cross-over end up with a large noodle in the centre (e.g. 3Dv1, 3Dv7) and subsequently both performed poorly in the analysis, which is consistent with [26] showing that the noodle is a critical damage area for composite T-joints under the same loading scenario. Increasing the proportion of yarn path entanglement can also improve the damage resistance capability. However, the noodle is still a critical failure region as yarn path entanglement does not change the noodle, so the damage resistance capability would not be enhanced as much as can be achieved by yarn path cross-over. On the contrary, increasing yarn path entanglement proportion leads to the reduction in straight yarns and therefore the structural stiffness would be compromised due to crimp introduced by the entangled weft yarns. Slightly reducing the yarn entanglement proportion was found to improve the stiffness of the T-joint whilst maintaining a similar load carrying capacity, which might be preferred in engineering applications.

8. Conclusions

The effect of fibre architecture variations on the mechanical performance of 3D woven T-joints under tensile pull-off loading was studied. Subjected to the existing preform manufacturing constraints, the weave design focuses on weft yarn path at the junction, where is the critical region for damage tolerance. There is still a tremendous amount of possible weave pattern variations even under this constraint. Therefore, two geometry-based design variables, i.e. proportions of weft yarn path entanglement and weft yarn path cross-over, were introduced to simplify the design space. Eight architecture designs of 3D woven T-joints based on different proportions of each design variable were evaluated and results were compared, and a significant variability was observed in the stiffness and load carrying capacity of these T-joints. In a design of experiments way, some of weave patterns were designed to show varying proportions of one design variable but with proportions of other variables maintaining unchanged. The influence of each single design variable was decoupled. Using yarn path cross-over was found to be an effective way to improve both stiffness and damage resistance. Increasing the proportion of yarn path entanglement can also improve the damage resistance capability. However, a high level of yarn path entanglement leads to a reduction in yarn path straightness and therefore the structural stiffness would be compromised due to the crimp introduced by the entangled weft yarns. Based on the above findings, design recommendations for 3D woven T-joint reinforcements under tensile pull-off loading were given.

Data availability

The raw/processed data required to reproduce these findings cannot be shared at this time as the data also forms part of an ongoing study.

Declaration of Competing Interest

The authors declare that they have no known competing financial interests or personal relationships that could have appeared to influence the work reported in this paper.

Acknowledgement

This work was supported by the Engineering and Physical Sciences Research Council [grant number EP/IO33513/1].

References

[1] Marsh G. Aero engines lose weight thanks to composites. Reinf Plast 2012;56(6):32–5.
[2] Cox BN, Dadkhah MS, Morris WL, Flintoff JG. Failure mechanisms of 3D woven composites in tension, compression, and bending. Acta Metall Mater 1994;42(12):3967–84.
[3] Turner P, Liu T, Zeng X. Collapse of 3D orthogonal woven carbon fibre composites under in-plane tension/compression and out-of-plane bending. Compos Struct 2016;142:286–97.
[4] Behera BK, Dash BP. Mechanical behavior of 3D woven composites. Mater Des 2015;67:261–71.
[5] Stig F, Hallstrom S. Assessment of the mechanical properties of a new 3D woven fibre composite material. Compos Sci Technol 2009;69(11–12):1686–92.
[6] Bandaru AK, Sachan Y, Ahmad S, Alagirusamy R, Bhatnagar N. On the mechanical response of 2D plain woven and 3D angle-interlock fabrics. Compos B Eng 2017;118:135–48.
[7] Lomov SV, Bogdanovich AE, Ivanov DS, Mungalov D, Karahan M. Verpoest I. A comparative study of tensile properties of non-crimp 3D orthogonal weave and multi-layer plain weave E-glass composites. Part 1: Materials, methods and principal results. Compos A Appl Sci Manuf 2009;40(8):1134–43.
[8] Dai S, Cunningham PR, Marshall S, Silva C. Influence of fibre architecture on the tensile, compressive and flexural behaviour of 3D woven composites. Compos A Appl Sci Manuf 2015;69:195–207.
[9] Saleh MN, Yudhanto A, Potluri P, Lubineau G, Soutis C. Characterising the loading direction sensitivity of 3D woven composites: Effect of z-binder architecture. Compos A Appl Sci Manuf 2016;90:577–88.
[10] Leong KH, Lee B, Herszberg I, Bannister MK. The effect of binder path on the tensile properties and failure of multilayer woven CFRP composites. Compos Sci Technol 2000;60(1):149–56.
[11] Umer R, Alhussein H, Zhou J, Cantwell W. The mechanical properties of 3D woven composites. J Compos Mater 2017;51(12):1703–16.
[12] Midani M, Seyam A-F, Saleh MN, Pankow M. The effect of the through-thickness yarn component on the in- and out-of-plane properties of composites from 3D orthogonal woven preforms. J Textile Inst 2018:1–11.
[13] Umair M, Hamdani STA, Asghar MA, Hussain T, Karahan M, Nawab Y, et al. Study of influence of interlocking patterns on the mechanical performance of 3D multilayer woven composites. J Reinf Plast Compos 2018;37(7):429–40.
[14] Castaneda N, Wisner B, Cuadra J, Amini S, Kontsos A. Investigation of the Z-binder role in progressive damage of 3D woven composites. Compos A Appl Sci Manuf 2017;98:76–89.
[15] Warren KC, Lopez-Anido RA, Goering J. Experimental investigation of three-dimensional woven composites. Compos A Appl Sci Manuf 2015;73:242–59.
[16] Brandt J, Drechsler K, Arendts FJ. Mechanical performance of composites based on various three-dimensional woven-fibre preforms. Compos Sci Technol 1996;56(3):381–6.
[17] Dahale M, Neale G, Lupicini R, Cascone L, McGarrigle C, Kelly J, et al. Effect of weave parameters on the mechanical properties of 3D woven glass composites. Compos Struct 2019;223:110947.
[18] Pankow M, Justusson B, Riosbaas M, Waas AM, Yen CF. Effect of fiber architecture on tensile fracture of 3D woven textile composites. Compos Struct 2019;225:111139.
[19] Soden JA, Weissenbach G, Hill BJ. The design and fabrication of 3D multi-layer woven T-section reinforcements. Compos A Appl Sci Manuf 1999;30(3):213–20.
[20] Yan S, Zeng X, Long A. Experimental assessment of the mechanical behaviour of 3D woven composite T-joints. Compos B Eng 2018;154:108–13.
[21] Yan S, Zeng X, Brown L, Long A. Geometric modeling of 3D woven preforms in composite T-joints. Text Res J 2017;88(16):1862–75.
[22] Yan S, Zeng X, Long A. Meso-scale modelling of 3D woven composite T-joints with weave variations. Compos Sci Technol 2019;171:171–9.
[23] Hashin Z. Failure criteria for unidirectional fiber composites. J Appl Mech-Trans ASME 1980;47(2):329–34.
[24] Caddell RM, Raghava RS, Atkins AG. Pressure dependent yield criteria for polymers. Mater Sci Eng 1974;13(2):113–20.
[25] Ruijter W. Analysis of mechanical properties of woven textile composites as a function of textile geometry. University of Nottingham; 2008.
[26] Cartié DDR, Dell'Anno G, Poulin E, Partridge IK. 3D reinforcement of stiffener-to-skin T-joints by Z-pinning and tufting. Eng Fract Mech 2006;73(16):2532–40.